Preparation and chemical deposition of pure and doped TiO$_2$ sols: application to nanocoatings for reactive gas cleaning

R. Azouani, L. Mokrani, M. Benmami, K. Chhor, J.-F. Bocquet, J.-L. Vignes, A. Kanaev [*]

Laboratoire d'Ingénierie des Matériaux et des Hautes Pressions, CNRS, Institut Galilée, Université Paris-Nord, 93430 Villetaneuse, France

We report on our recent progress in preparation of pure and N-doped TiO$_2$ nanocoatings for reactive gas cleaning. The oxo-particles are generated in the sol-gel reactor with rapid reagent mixing, temperature and atmosphere control. Their size is monitored *in situ* by light scattering method using optical-fibre probe. The N-doping is achieved during the particle nucleation stage. An ultra-thin surface coverage is achieved during a short contact time between the chemically active sols and a support. The coatings are then treated at 450°C during 4h. They are mechanically stable and exhibit high photocatalytic activity in both UV and visible spectral ranges.

I. Introduction

A knowledge and nano-scale control of dispersed solids preparation is expected to largely contribute in attaining of optimal useful material properties. Adequate methods of nanoparticles preparation and immobilization may therefore open perspectives for successful large-scale applications.

This is a case of TiO$_2$ issued of sol-gel synthesis, where reactive oxo-clusters and nanoparticles (nuclei) appear at the initial stage of the process (Monticone et al., 1999; Soloviev et al., 2001a-b). The colloids are metastable and solid precipitates after the so-called induction time, that critically depends on the titanium tetraisopropoxyde (TTIP) precursor concentration C_{Ti} and hydrolysis ratio $H=C_W/C_{Ti}$, where C_W is water concentration: $t_{ind} \propto C_{Ti}^{-6}(H-1.45)^{-5}$ (Soloviev et al., 2003). The growth kinetics is explained by condensation reactions between surface hydroxyl groups of particles (Rivallin et al., 2004).

In our approach we avoid nanoparticle stabilization by chemical additives, as this decreases the reactivity and result in poor particle coupling to substrates. This, in turn, worsens mechanical stability and lifetime of the resulted coatings as well as decrease charge-separation efficiency, which is of importance for photocatalysts.

In order to achieve the sol-gel process control, we have developed a reactor based on rapid reagents micro-mixing and in situ particle-size measurements by light-scattering methods (Rivallin 2003a; Rivallin et al., 2005). This reactor assures reproducibility of the process kinetics within 5% and allows generation of the monodispersed nuclei.

Under controlled experimental conditions the lifetime of produced TiO$_2$ clusters and particles can be long enough to enable steady-state observations. However, they are

---

[*] Correspondent author. E-mail: kanaev@limhp.univ-paris13.fr

extremely chemically active, in particularly subjecting condensation reactions with surface hydroxyl groups. This behavior has been used for nanoparticles elaboration and immobilisation in the sol-gel reactor. A control of the elementary units stability and their reaction kinetics allowed realization of nanocoatings on complex-shape substrates for applications in surface protection and environmental photocatalysis (Benmami et al., 2005a-b; 2006a-b). Efficient impregnation of TiO_2 nanoparticles into the nanoporous silica granular has been successfully realized by Pucher et al. (2007) for gas-cleaning technologies. The same approach enables efficient and homogeneous doping of TiO_2 as recently shown by Benmami et al. (2006c).

In the present communication we address to the reactive clusters and particle doping with the aim to extend the catalyst working range to the visible. The N-doping has been proposed by Asahi et al. (2001) and experimentally developed in many recent studies. We propose an original method of *dynamical* doping of TiO_2 reactive clusters and nanoparticles appearing at nucleation stage. This doping can offer a better dopant integration into the bulk TiO_2 solid. A nano-scale process control is required for elaboration of efficient nanocoatings.

II. Experiment and Discussion

Sols preparation

The nanoparticles are generated in the sol-gel reactor described in details by Rivallin et al. (2005). Its main part is the T-mixer (Hartridge and Roughton, 1923) schematically shown in Fig. 1. Two thermostatic stock solutions (T=5-30°C ±0.02°C, cryostat HAAKE DC10k-15) TTIP/2-propanol and water/2-propanol are injected into the mixer trough two input tubes. The injection is exocentric: two fluids form a vortex before entering the main tube. The reagents flow rates are maintained

Fig. 1 : T-mixer

equal and varying from 2 to 12 m/s by applying the external gas pressure (N_2). The diameters (d) of two input (1.0 mm) and the main (2.0 mm) tubes are chosen to conserve the Reynolds number, Re=$4Q\rho/\pi\eta d$, where Q, ρ, and η are the fluid flow rate, density and dynamic viscosity. In the experimental conditions the Reynolds number varied from 1000 to 8000. The process was conducted at C_{Ti}=0.146M, T=20°C, and at different $1\leq H\leq 2.5$.

The particle population is controlled by a fibre-optical probe coupled to 10-W He-Ne laser (emitter fibre) and photomultiplier (receiver fibre). It allows simultaneous measurements of the mean hydrodynamic radius R (as small as ~1.0 nm) and total light intensity scattered of particles (I). Advantage of using this probe is that it allows working in reactors with non-transparent walls, moderately agitated solutions (Rivallin et al., 2003b) and it weakens constraints related to multiple scattering phenomenon, due to a small observation volume of 10^{-4}-10^{-5} cm^3. The photomultiplier signal in the photon counting mode is proceeded by a digital UNICOR correlator developed by Yudin et al. (1997).

As shown in previous studies of nanoparticles precipitation (Schwarzer et al., 2004; Gradl et al., 2006; Marchisio et al., 2006), the fluid flow in T-mixer is turbulent in these conditions. A decrease of the fluids micromixing time can be decreased below the
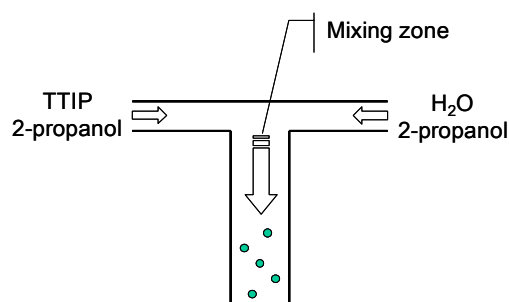
reaction time, which results in the particle nucleation. Working at small Damköhler numbers Da≤1 allows advanced fluid homogenizing resulting in smaller size and narrower size distribution, which are of importance for applications in photocatalysis (Marugan et al., 2006).

Adequate choice of the injection flow rate depends on the fluid reactivity. In particularly, studying barium sulfate precipitation at room temperature, Marchisio et al. (2006) have shown a strong decrease of the

Fig. 2 : Kolmogorov length (L_K) and mean particle size (R) as a function of Re number.

BaSO$_4$ particle size at Re≥1000. The mean particle size in these studies was R≥50 nm.

In contrast, our sol particles are considerably smaller. The sol-gel synthesis based on TTIP precursor is extremely sensitive to the reagent concentrations. In typical experimental conditions the basic hydrolysis-condensation reactions are rapid and primary clusters and nanoparticles appears on the time-scale of tens of milliseconds (Livage and Sanchez, 1998). This makes important the study of sol-gel process.

At long mixing time, the basic colloid is strongly polydispersed. However when the flow rate increases, the particle size and polydispersity decrease. We have observed this kinetics crossover at the Reynolds number Re≈4400. The dependence of the Kolmogorov length (L_K) and the mean particle size R on Reynolds number is shown in Fig. 2. One can see that the minimal mean particle size is attained at L_K≤3 μm. The mixing time t_m=8 ms corresponding to Re=4400 can be obtained from the calibration experiments by Rivallin (2003a): t_m=11-6.9·10^{-4}×Re. Assuming Damköhler number Da~1 in these conditions, we estimate the characteristic time of hydrolysis-condensation reactions leading to nucleation τ~10^{-2} s at C_{Ti}=0.146 M and H=2.0.

Fig. 3 shows two *pseudo* particle-size distributions measured at Re=1000 and 6000. It is measured as independent series with observation in a small volume of ~10^{-5} cm^3 during a short time of 60 s. The particle size is then calculated from fit of the auto-correlation function curves (ACF). The histogram of these measurements reflects two factors: (i) true fluctuations of particle size in the observation volume and (ii) apparent fluctuations due to a limited series length. In the limit of the monodispersed particles, the second factor defines the population dispersion.

As one can see from Fig. 3, the size distribution at Re=1000 (R=3.2 nm) is twice larger than that at Re=6000 (R=2.0 nm). We relate this difference to the net effect of the particle size. On the other hand, we believe that in the limit of large Re>4500 the colloids are almost monodispersed and the dispersion is due to a poor data statistics. This approach doesn't allow obtaining the true size
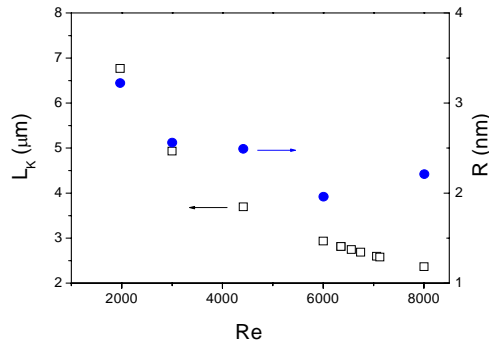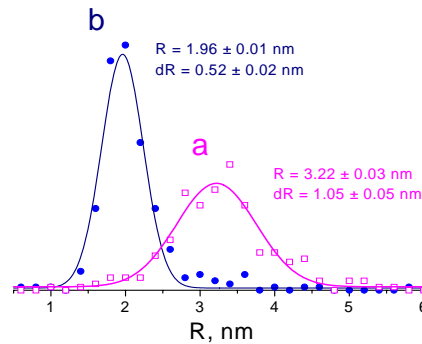

Fig. 3 : Particle size distributions for injection at Re=1000 (a) and 6000 (b). Gaussian fits are shown by solid lines.

distribution, however displays a tendency to its variation.

Our experiments show that different cluster and particle size can be produced in the reactor depending on process parameters. An example of ACF curves of sols obtained at different H (Re=6000) is shown in Fig. 4. The fit of these data suggests quasi monodispersed size distributions. The particle size obtained from this fit is 2R=2.0 nm for H=1.35, 3.2 nm for H=1.75, and 5.0 nm for H=2.0. This possibility of temporal stabilization of extremely reactive TiO_2 clusters and particles enables efficient doping and deposition processes.

Doping

The doped N_xTiO_{2-x} sols have been obtained in present studies by dissolving hydroxyurea in H_2O/2-propanol solution until the saturation, before entering the

Fig. 4 : ACF of nanoparticles at different hydrolysis ratios H.

reactive mixing stage. At fluids contact in the T-mixer (Fig. 1) hydrolysis-condensation reactions leading to TiO_2 nucleation and TiO_2-cluster reactions with the dopant molecules proceed simultaneously. The prepared colloid exhibits light yellow color. The rates adjustment between these two reaction channels can be achieved by varying the hydrolysis ratio H. We have used for doping three solutions prepared at H=1.0, 1.5 and 2.5 that according to our results show the mean particle size of 2R=1.9, 3.2 and 2.5 nm. This allowed inspecting the effect of doping as a function of size. The chemical analysis of as-prepared sols indicates a mean nitrogen mass loading ~0.7%.

Coating preparation

The method of chemical nanocoating preparation has been described by Benmami et al. (2005a-b; 2006a-c). We have used as support 1-mm glass beads transparent to both visible and UV ($\lambda \geq 320$ nm) light. Before coating, the beads were treated in acid solution and ultrasound bath. The nanocoatings are achieved by support introduction into the reactor bath set at the T-mixer output. A short contact time is required to avoid particle precipitation resulting in inactive coatings (Benmami et al., 2005b; 2006a). The substrates were then separated from the reactive colloid in dry atmosphere and the liquid layer (containing excessive non-reacted nanoparticles) was removed from their surface. After drying at 80°C, the substrates were thermally treated at 450°C during 4h that assures appearance of the most photocatalytically efficient anatase-amorphous TiO_2 phase (Benmami, 2006d). The BET surface of nanocoating measured by Coulter SA3100 setup before and after thermal treatment was 380 m^2/g and 98 m^2/g respectively. These values are close to those earlier reported for non-doped TiO_2 nanocoatings (Benmami et al., 2005b; 2006a). Mass loading of immobilised catalysts on the glass beads were obtained using ammonium sulphate (NH_4SO_4) - sulphuric acid (H_2SO_4) digestion as described by Coronado et al. (2003). We have measured the deposited mass of titanium oxide sols of ≤ 1 mg/g of 1-mm glass beads. This corresponds to a thickness of the deposited layer $\delta \leq 100$ nm. The UV absorption of our N-doped TiO_2 nanocoatings is generally low due to a small deposited mass. In the same
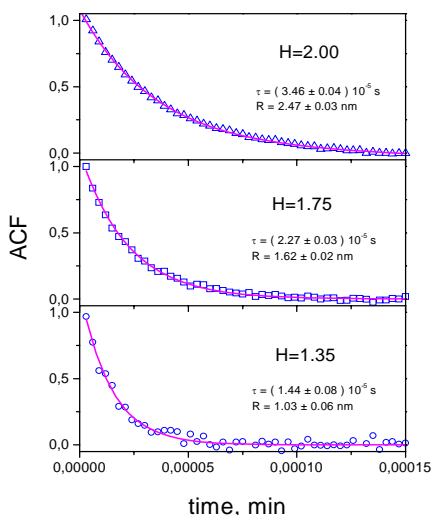
time, they exhibit extended absorption in the visible spectral range up to ~570 nm (Benmami, 2006c).

For a comparison, Degussa P25 coated glass beads were also prepared as described by Benmami et al. (2005b). Their deposited mass was >5.2 mg/g of the glass beads.

Photocatalytic performance of nanocoatings

The photocatalytic performance of N-doped TiO_2 nanocoatings has been studied in a fix-bed reactor described elsewhere (Benmami et al., 2005a-b, 2006a). The trichloroethylene (TCE) has been used as a model pollutant at concentration ~400 ppm. Atmospheric air at p≈1 bar of ~10% relative humidity at 20°C was used as a carrier gas. The pollutant passes through a reactor tube of 6-mm diameter filled with N-TiO_2 covered glass beads. The gas mixture flow was maintained at 250 cm^3/min by mass flow meters (Brooks). Six 8-W lamps of two types were positioned around the reactor tube: UV lamps emitting at λ=362±11 nm (UV1) and broadband UV-visible lamps with maximum spectral intensity at ~500 nm (VIS2). The residence time of the pollutant in the irradiated zone of 2.5-cm length was ~0.1 s. The concentrations of the pollutant before and after the photocatalytic reactor were monitored by the gas chromatography method (HP 5880 series). The reactor temperature measured by K-thermocouple (chromel/alumel) did not exceed 45°C.

The photocatalytic performance of pure TiO_2 nanocoatings, both amorphous and crystalline, has been reported by Benmami et al. (2005a-b) and Benmami (2006d). Here we present photocatalytic tests of new N-doped nanocoatings. The results are shown in Fig. 5 under UV1 (a) and VIS2 (b) lamp illumination.

The reactor yield has been calculated as $Y=(A_0-A)/A_0×100\%$, where A_0 and A are correspondingly the TCE pollutant concentrations before and after the reactor. The lamp on/off cycles are separated in Fig. 5 by dotted lines.

The Y(t) rapidly increases as the irradiation starts before a stationary performance is attained. However, the transient time is shorter with the UV irradiation compared to the visible one. The reason of that is not yet clear.

All nanocoatings show strong visible activity. However, one can remark that nanocoating prepared at H=1.5 is 30% more efficient compared to those prepared at H=1.0 and H=2.5. This may be the effect of size of the TiO_2 oxo-clusters on the doping process. The UV performance of the nanocoatings appears to be comparable to that of
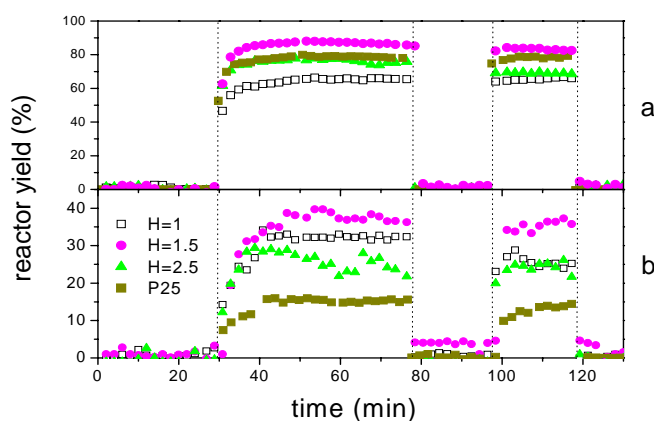

Fig. 5 : Photocatalytic yield of the TCE degradation of the N-doped TiO_2 at UV1 (a) and VIS2 (b) lamp irradiations. TCE decomposition rate $r∝ln(1-Y/100\%)$, assuming first order kinetics.

the Degussa P25 catalyst. As our results show, the TCE decomposition rate using Degussa P25 decreases 10 times when replacing UV1 lamps by VIS2. This corresponds to the VIS2-lamps contribution to UV: $\lambda \leq 400$ nm. Keeping in mind this factor, one can conclude about generally lower activity of the N-doped nanocatalyst when activated by visible photons instead of UV ones. The quantum efficiency of the nanocoatings (defined as $\gamma = N_{TCE}/N_{ph}$, where N_{TCE} and N_{ph} are correspondingly numbers of the reacted TCE molecules and absorbed photons) under UV illumination may be however higher than that of the Degussa P25 because of their much smaller mass. The visible activity of the N-doped TiO_2 nanocoatings is much higher then that of Degussa P25.

III. Conclusion

We report on preparation and photocatalytic activity of N-doped TiO_2 nanocoatings in the sol-gel reactor with rapid reagent mixing and temperature and atmosphere control. The doping is achieved during the particles nucleation stage. The prepared catalyst shows strong activity under visible light illumination. Moreover, our results show 30% higher activity of the coatings prepared at the hydrolysis ratio H=1.5 compared to H=1.0 and 2.5. The size of TiO_2 clusters subjected to doping may be responsible for this effect.

IV. Acknowledgments

References

Asahi R., Morikawa T., Ohwaki T., Aoki K., Taga Y., 2001, Science 293, 269.

Benmami M., Chhor K., Kanaev A., 2005a, AIDIC Conf. Ser., 7, 29.

Benmami M., Chhor K., Kanaev A., 2005b, J. Phys. Chem. B 109, 19766.

Benmami M., Chhor K., Kanaev A., 2006a, Chem. Phys. Lett. 422, 552.

Benmami M., Kanaev A. V., Vignes J. L., Beauverger M., Amamra M.C., Chhor K., 2006b, Proc. Matériaux-06 (Dijon, France).

Benmami M., Kanaev A.V., Vrel D., Lay L., Bocquet J.F, Chhor K., 2006c, Proc. Matériaux-06 (Dijon, France).

Benmami, 2006d, PhD thesis, University Paris 13.

Coronado J. M., Zorn J. M., Tejedor-Tejedor I., Anderson M., 2003, Appl. Catal. B: Environ. 43, 329.

Gradl J., Schwarzer H.-C., Schwertfirm F., Manhart M., Peukert W., 2006, Chem. Eng. Proc. 45, 908.

Hartridge H. and Roughton F. J. W., 1923, Proc. Roy. Soc. London, A 104, 376.

Livage, J., Henry M. and C. Sanchez, 1998, Prog. Solid. Stat. Chem., 18, 259.

Marchisio D.L., Rivautella L., Barresi A.A., 2006, AIChE J. 52, 1877.

Marugan J., Hufschmidt D., Sagawe G., Selzer V., Bahnemann B., 2006, Water Res. 40, 833.

Monticone S., Soloviev A., Tufeu R. and Kanaev A. V., 1999, AIDIC Conf. Ser. 4, 77.

Pucher P., Benmami M., Krammer G., Chhor K., Bocquet J.-F., Kanaev A., 2007, Proc. Partec-07 (Nuremberg, Germany).

Soloviev A., Tufeu R., Ivanov D. and Kanaev A., 2001a, J. Mater. Sci. Letters, 20, 905.

Soloviev A., Tufue R., Sanchez C. and Kanaev A., 2001b, J. Phys. Chem. B 105, 4175.

Soloviev A., Jensen H., Søgaard E. G. and Kanaev A. V., 2003, J. Mater. Sci., 38, 3315.

Rivallin, M., 2003a, PhD thesis, ENSMP, Paris, France.

Rivallin M., Gaunand A. and Kanaev A., 2003b, Chem. Eng. Trans. 3, 919.

Rivallin M., Benmami M., Gaunand A. Kanaev A., 2004, Chem. Phys. Lett. 398, 157.

Rivallin M., Benmami M., Kanaev A., Gaunand, A., 2005, Chem. Eng. Res. Des. 83(A1), 1.